

**\*\*Volume Title\*\***  
*ASP Conference Series, Vol. \*\*Volume Number\*\**  
**\*\*Author\*\***  
 © **\*\*Copyright Year\*\*** *Astronomical Society of the Pacific*

## Pair-Instability Supernovae of Non-Zero Metallicity Stars

Ke-Jung Chen<sup>1,2,\*</sup>, Alexander Heger<sup>2,3,4</sup>, Stan Woosley<sup>1</sup>, Ann Almgren<sup>5</sup> and Daniel J. Whalen<sup>6</sup>

<sup>1</sup>*Department of Astronomy & Astrophysics, University of California, Santa Cruz, CA 95064, USA*

<sup>2</sup>*School of Physics and Astronomy, University of Minnesota, Minneapolis, MN 55455, USA*

<sup>3</sup>*Monash Centre for Astrophysics, Monash University, Victoria 3800, Australia*

<sup>4</sup>*Joint Institute for Nuclear Astrophysics, University of Notre Dame Notre Dame, IN 46556 USA*

<sup>5</sup>*Center for Computational Sciences and Engineering, Lawrence Berkeley National Lab, Berkeley, CA 94720, USA*

<sup>6</sup>*Zentrum für Astronomie, Institut für Theoretische Astrophysik, Universität Heidelberg, Albert-Ueberle-Str. 2, 69120 Heidelberg, Germany*

*\*IAU Gruber Fellow; kchen@ucolick.org*

### Abstract.

Observational evidence suggests that some very massive stars in the local Universe may die as pair-instability supernovae. We present 2D simulations of the pair-instability supernova of a non-zero metallicity star. We find that very little mixing occurs in this explosion because metals in the stellar envelope drive strong winds that strip the hydrogen envelope from the star prior to death. Consequently, a reverse shock cannot form and trigger fluid instabilities during the supernova. Only weak mixing driven by nuclear burning occurs in the earliest stages of the supernova, and it is too weak to affect the observational signatures of the explosion.

### 1. Introduction

The fate of a massive star is determined by its initial mass, composition, and mass loss over its life (which is still poorly understood). The explosion mechanism and remnant properties is mainly determined by the helium core mass when the star dies. Kudritzki (2002) suggests that the mass loss rate of a star,  $\dot{m}$ , is  $\propto Z^{0.5}$ , where  $Z$  is the metallicity of the star relative to the solar metallicity,  $Z_{\odot}$ . Since the first (or Pop III) stars form in pristine H and He gas, it is generally thought that they retain most of their mass over their lifetimes. Pop III stars above  $80 M_{\odot}$  encounter the pair production instability after central carbon burning, in which large numbers of thermal photons create  $e^{-}/e^{+}$  pairs at the expense of pressure support in the core. If Pop III stars are over  $150 M_{\odot}$  but less than  $260 M_{\odot}$ , core contraction due to the loss of pressure support to pair production ignites explosive oxygen and silicon burning that results in an energetic explosion that

completely unbinds the star. This thermonuclear explosion is called a pair-instability supernova (PSN; Barkat et al. 1967; Heger & Woosley 2002; Chen 2014; Chen et al. 2014a,b). A PSN can explode with up to  $10^{53}$  erg of energy, or about 100 times that of a Type Ia SN. Explosive silicon burning can synthesize up to  $40 M_{\odot}$  of  $^{56}\text{Ni}$  in these events which, along with their large explosion energies, makes them extremely bright. PSNe are therefore visible at high redshifts and could be used to probe the properties of the first stars (Kasen et al. 2011; Whalen et al. 2013c,a; Pan et al. 2012). Isotopes heavier than the iron group are completely absent from the chemical yields of PSNe because of the absence of neutron capture processes (r- and s-processes). The important question arises : Can the most massive stars in the local Universe also die as PSNe? If so, how do these PSNe differ from those of Pop III progenitors?

The detection of PSN candidates SN 2007bi and SN 2213 - 1745 (Gal-Yam et al. 2009; Cooke et al. 2012) has increased interest in PSNe and poses a challenge to theories of galactic star formation, because how progenitors so massive can form at metallicities of  $0.1 Z_{\odot}$  today is very unclear. Stars at these metallicities can easily lose most of their mass over their lifetimes to strong stellar winds, and so they must form at even higher masses than Pop III stars to die as PSNe. Understanding the observational signatures of PSNe at near-solar metallicities is key to identifying and properly interpreting these events as more are discovered. To date, PSN models have focused on Pop III stars. In this paper, we present 2D simulations of a PSN of a non-zero metallicity star and investigate if mixing can affect explosive burning or observational signatures. We first describe our numerical methods and problem setup in § 2. Our results are discussed in § 3, and our conclusions are given in § 4.

## 2. Methodology & Problem Setup

Self-consistent multidimensional stellar evolution models from the onset of hydrogen burning to eventual core collapse and explosion remain beyond the realm of contemporary computational power. We instead initialize our multidimensional explosion simulation with a  $500 M_{\odot}$   $0.1 Z_{\odot}$  star that is evolved from the zero-age main sequence to the onset of core collapse in the 1D stellar evolution code GENEVA (Hirschi et al. 2004; Whalen et al. 2013b). Our model includes mass loss and stellar rotation to determine the final structure of the star. The initial rotational velocity is 40% of the critical velocity, or a surface velocity of 450 km/sec at the equator. The star is evolved up to the onset of explosive oxygen burning, about 10 s before maximum core contraction. Initializing this profile in a 2D simulation at this time should therefore capture instabilities seeded by both collapse and explosive burning. The explosion time scale is about tens of seconds which is much shorter than the rotational period of star,  $P \sim$  several hours. It is reasonable to assume that the star is non-rotating during the explosion phase, so we neglect the effect of rotation in the 2D simulation.

We map the 1D profile of the star to a 2D cylindrical coordinate grid in  $r$  and  $z$  in CASTRO with the conservative mapping scheme of Chen et al. (2013). CASTRO is a multidimensional adaptive mesh refinement (AMR) astrophysical radiation hydrodynamics code (Almgren et al. 2010; Zhang et al. 2011). It has a higher-order unsplit Godunov hydro scheme and block-structured AMR. In our models we use the Helmholtz EOS (Timmes & Swesty 2000) for stellar matter, which includes degenerate and non-degenerate, relativistic and non-relativistic electrons, electron-positron pair production, and an ideal gas with radiation. CASTRO evolves mass fractions for each isotope with

its own advection equation. The monopole approximation is used for self-gravity, in which a 1D gravitational potential is constructed from the radial average of the density and then differenced to construct the gravitational force vector everywhere in the AMR hierarchy. This approximation is well-suited to the nearly spherical symmetry of the star and is efficient. We use the 19-isotope APPROX nuclear reaction network (Weaver et al. 1978; Timmes 1999), which includes heavy-ion reactions, alpha-chain reactions, hydrogen burning cycles, photo-disintegration of heavy nuclei, and energy loss through thermal neutrinos. Nuclear burning is self-consistently coupled to hydrodynamics, and we also account for energy deposition due to radioactive decay of  $^{56}\text{Ni} \rightarrow ^{56}\text{Co} \rightarrow ^{56}\text{Fe}$ .

The grid size is  $4 \cdot 10^{10} \times 4 \cdot 10^{10} \text{ cm}^2$ , with 256 uniform zones in both  $r$  and  $z$ . Up to three levels of refinement, each with a factor of 4 greater resolution, are permitted throughout the simulation. The resolution at the finest level is  $2 \times 10^7 \text{ cm}$ , which is sufficient to resolve the characteristic scales of nuclear burning ( $\sim 10^8 \text{ cm}$ ). The grid is refined on functions of the gradients in density, velocity, and pressure. Because we only simulate one octant of the star, we apply reflecting boundary conditions at the inner  $r$  and  $z$  boundaries; we impose outflow boundary conditions on the upper boundaries. Refined grids are nested around the core of the star to assure that it is always at the highest resolution. We evolve our simulations until the shock breaks through the surface of the star.

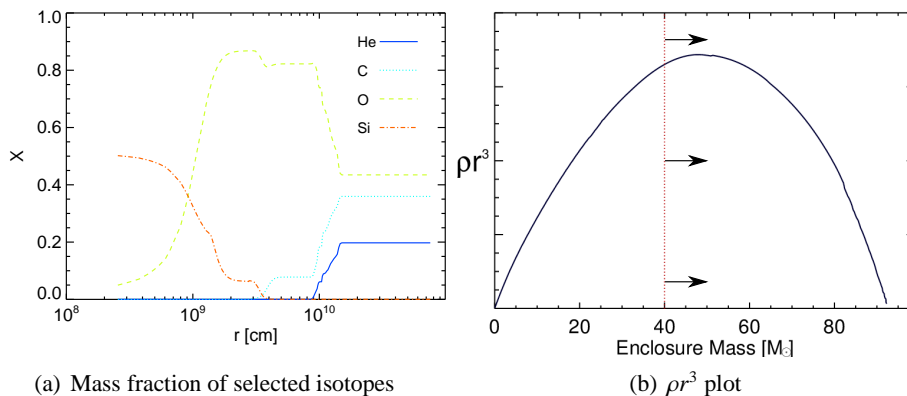


Figure 1. Left: isotope mass fractions. The high silicon mass fraction at the core shows that oxygen burning is complete. Right: plot of  $\rho r^3$ . The bump at the center is due to the helium core. The red dashed line marks the approximate site of the formation of the shock. The shock propagates only a short distance through a region of increasing  $\rho r^3$ , so it is unlikely to decelerate and create a reverse shock or therefore fluid instabilities.

### 3. Results

The mass of the star falls from  $500 M_\odot$  to  $92.5 M_\odot$  over its lifetime because of stellar winds and rotation. Strong winds not only remove the hydrogen envelope but also strip away the outer layer of the helium core. The central temperature and density of the core when it has begun to contract are  $3.31 \times 10^9 \text{ K}$  and  $1.24 \times 10^6 \text{ g cm}^{-3}$ . In Figure 1(a) we show mass fractions for helium, carbon, oxygen, and silicon at the end of the GENEVA

simulation. The oxygen is nearly depleted, and explosive silicon burning is about to begin because of runaway core contraction. Explosive silicon burning begins soon after the CASTRO run is launched, after a brief phase of further contraction. Burning releases  $3.33 \times 10^{52}$  ergs and synthesizes  $3.63 M_{\odot}$  of  $^{56}\text{Ni}$ . The star is completely disrupted, leaving no compact object behind. This large  $^{56}\text{Ni}$  mass can power the PSN light curve for several months. If fluid instabilities dredge  $^{56}\text{Ni}$  up from greater depths, it could affect luminosities at intermediate times. We plot oxygen and  $^{56}\text{Ni}$  mass fractions 10 s after core bounce in Figure 2(a). Moderate fluid instabilities driven by nuclear burning are visible at the inner boundary of the oxygen shell, but mixing is limited. The  $^{56}\text{Ni}$  essentially remains untouched by dynamical instabilities.

The explosion drives a strong shock with initial velocities of  $2 - 3 \times 10^9$  cm/s. Because the radius of the star is only  $\sim 3 \times 10^{10}$  cm, the shock reaches its surface in under 20s. Breakout happens at a much smaller radius than in Pop III PSNe ( $10^{12} - 10^{13}$  cm). We show densities and oxygen abundances at shock breakout in Figure 2(b). The SN ejecta remains roughly spherical in density and O mass fraction, indicating there is not much mixing during the explosion. There are no prominent signs of mixing during collapse, burning or subsequent expansion. The reason for this can be found in the plot of  $\rho r^3$  in the right panel of Figure 1. The shock decelerates in regions of increasing  $\rho r^3$  as it plows up mass, and could form a reverse shock that is prone to Rayleigh-Taylor (RT) instabilities. But Figure 1(b) shows that when the SN shock forms it is nearly out of the region of increasing  $\rho r^3$ , so there is little time for RT instabilities, or mixing, to occur.

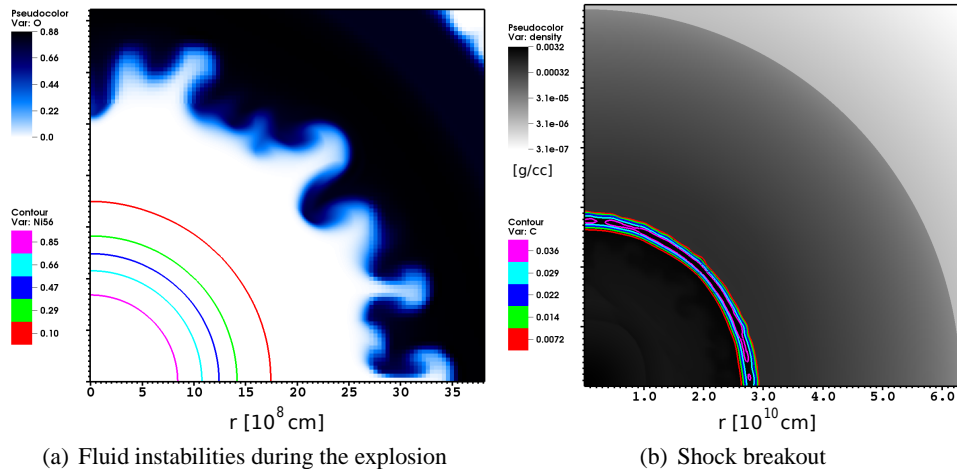


Figure 2. Left: oxygen and  $^{56}\text{Ni}$  mass fractions.  $^{56}\text{Ni}$  mass fractions within the red arc are greater than 0.1. The inner region of the oxygen-burning shell shows only mild mixing during explosive burning that does not reach the  $^{56}\text{Ni}$  layer. Right: densities (gray) and carbon abundance (contours). The SN ejecta is fairly spherical, and there is no evidence of mixing in density or mass fractions of carbon.

#### 4. Conclusions

We have examined mixing in the PSN explosions of compact non-zero metallicity stars. We find that only mild fluid instabilities form during the explosion and do not result in visible mixing at shock breakout. This is primarily due to the fact that RT instabilities do not have time to form before the shock breaks out of the compact star, which is essentially a bare He core. In this sense, such explosions may be similar to Pop III PSNe of blue progenitors. Our model has an explosion energy and  $^{56}\text{Ni}$  yield that is similar to the  $200 M_{\odot}$  Pop III PSN in Chen et al. (2014a).

The formation of a  $500 M_{\odot}$  star at near-solar metallicities is a challenge to current theories of present-day star formation. Radiation from the star normally halts accretion well before the star reaches such masses. Mergers between stars in dense clusters in principle could build up stars of up to several hundred solar masses. If so, dense star clusters could be promising sites for hunting for pair-instability supernovae in the local Universe.

**Acknowledgments.** KC thanks the members of the CCSE at LBNL for help with CASTRO. This work was supported by the IAU-Gruber Fellowship, Stanwood Johnston Fellowship, and KITP Graduate Fellowship. Work at UCSC has been supported by the DOE HEP Program under contract de-sc0010676; the National Science Foundation (AST 0909129) and the NASA Theory Program (NNX09AK36G). AH acknowledges support by an ARC Future Fellowship (FT120100363) and a Monash University Larkins Fellowship. DJW acknowledges support from the European Research Council under the European Community's Seventh Framework Programme (FP7/2007-2013) via the ERC Advanced Grant "STARLIGHT: Formation of the First Stars" (project number 339177). All numerical simulations were done with allocations from the University of Minnesota Supercomputing Institute and the National Energy Research Scientific Computing Center.

#### References

- Almgren, A. S., Beckner, V. E., Bell, J. B., Day, M. S., Howell, L. H., Joggerst, C. C., Lijewski, M. J., Nonaka, A., Singer, M., & Zingale, M. 2010, *ApJ*, 715, 1221.
- Barkat, Z., Rakavy, G., & Sack, N. 1967, *Physical Review Letters*, 18, 379.
- Chen, K.-J. 2014, *International Journal of Modern Physics D*, 23, 1430008.
- Chen, K.-J., Heger, A., & Almgren, A. S. 2013, *Astronomy and Computing*, 3, 70.
- Chen, K.-J., Heger, A., Woosley, S., Almgren, A., & Whalen, D. J. 2014a, *ApJ*, 792, 44.
- Chen, K.-J., Woosley, S., Heger, A., Almgren, A., & Whalen, D. J. 2014b, *ApJ*, 792, 28.
- Cooke, J., Sullivan, M., Gal-Yam, A., Barton, E. J., Carlberg, R. G., Ryan-Weber, E. V., Horst, C., Omori, Y., & Díaz, C. G. 2012, *Nat*, 491, 228.
- Gal-Yam, A., Mazzali, P., Ofek, E. O., Nugent, P. E., Kulkarni, S. R., Kasliwal, M. M., Quimby, R. M., Filippenko, A. V., Cenko, S. B., Chornock, R., Waldman, R., Kasen, D., Sullivan, M., Beshore, E. C., Drake, A. J., Thomas, R. C., Bloom, J. S., Poznanski, D., Miller, A. A., Foley, R. J., Silverman, J. M., Arcavi, I., Ellis, R. S., & Deng, J. 2009, *Nat*, 462, 624.
- Heger, A., & Woosley, S. E. 2002, *ApJ*, 567, 532.
- Hirschi, R., Meynet, G., & Maeder, A. 2004, *A&A*, 425, 649.
- Kasen, D., Woosley, S. E., & Heger, A. 2011, *ApJ*, 734, 102.
- Kudritzki, R. P. 2002, *ApJ*, 577, 389.
- Pan, T., Kasen, D., & Loeb, A. 2012, *MNRAS*, 422, 2701.
- Timmes, F. X. 1999, *ApJS*, 124, 241.
- Timmes, F. X., & Swesty, F. D. 2000, *ApJS*, 126, 501.

- Weaver, T. A., Zimmerman, G. B., & Woosley, S. E. 1978, *ApJ*, 225, 1021.
- Whalen, D. J., Even, W., Frey, L. H., Smidt, J., Johnson, J. L., Lovekin, C. C., Fryer, C. L., Stiavelli, M., Holz, D. E., Heger, A., Woosley, S. E., & Hungerford, A. L. 2013a, *ApJ*, 777, 110.
- Whalen, D. J., Even, W., Smidt, J., Heger, A., Hirschi, R., Yusof, N., Stiavelli, M., Fryer, C. L., Chen, K.-J., & Joggerst, C. C. 2014b, *ApJ*, 797, 9.
- Whalen, D. J., Fryer, C. L., Holz, D. E., Heger, A., Woosley, S. E., Stiavelli, M., Even, W., & Frey, L. H. 2013c, *ApJ*, 762, L6.
- Zhang, W., Howell, L., Almgren, A., Burrows, A., & Bell, J. 2011, *ApJS*, 196, 20.